THE ASTROPHYSICAL JOURNAL, 401:220–225, 1992 December 10

FAR-ULTRAVIOLET OBSERVATIONS OF THE SUPERNOVA REMNANT N49 USING THE HOPKINS ULTRAVIOLET TELESCOPE

OLAF VANCURA,[1] WILLIAM P. BLAIR,[1] KNOX S. LONG,[1,2] ARTHUR F. DAVIDSEN,[1] CHARLES W. BOWERS,[1]
W. VAN DYKE DIXON,[1] SAMUEL T. DURRANCE,[1] PAUL D. FELDMAN,[1] HENRY C. FERGUSON,[3]
RICHARD C. HENRY,[1] RANDY A. KIMBLE,[4] GERARD A. KRISS,[1]
JEFFREY W. KRUK,[1] AND H. WARREN MOOS[1]

Received 1992 February 24; accepted 1992 June 17

ABSTRACT

Using the Hopkins Ultraviolet Telescope on the *Astro-1* space shuttle mission in 1990 December, we have obtained a far-ultraviolet spectrum (912–1860 Å at 3.5 Å resolution) of a complex of bright filaments located in the eastern part of the supernova remnant N49 in the Large Magellanic Cloud. This is the first observation of an extragalactic supernova remnant that extends to the Lyman limit. We detect lines of O VI λ1035, O IV] λ1403, C IV λ1550, and He II λ1640. The O VI emission that we observe cannot originate in shocks with velocities $\lesssim 140$ km s^{-1} which are responsible for the bulk of both the C IV and the optical line emission. Likewise, the main blast wave with a velocity ~ 730 km s^{-1} is unable to account for the brightness of O VI. Most of the O VI originates in optically faint, 190–270 km s^{-1} shocks, traversing clouds with densities of 20–40 cm^{-3}. We expand upon earlier modeling of N49 *IUE* and optical spectra that assumed a distribution of shock velocities; including data from below Lyα, such models still describe the data well.

Subject headings: ISM: individual (N49) — Magellanic Clouds — shock waves — supernova remnants — ultraviolet: interstellar

1. INTRODUCTION

Mathewson, Healey, & Westerlund (1963) first identified N49 as a supernova remnant (SNR) based on its nonthermal radio emission. N49 is the highest optical surface brightness SNR in the Large Magellanic Cloud (LMC) (Dopita 1979) and is the third brightest X-ray SNR (Long, Hefland, & Grabelsky 1981). At a distance of 50 kpc (Eastman & Kirshner 1989), N49's angular diameter of $\sim 1'$ corresponds to a physical diameter of ~ 16 pc. Age estimates range from 5000 to 16,000 yr (Long et al. 1981; Shull 1983; Vancura et al. 1992, hereafter VBLR). The reddening along the line of sight to N49 averages $E(B-V) \simeq 0.37$ but varies on scales as small as 2″ (Dennefeld 1986; VBLR). Except for its positional association with a γ-ray burst source (Cline et al. 1982) and its high surface brightness, N49 appears typical of other middle-aged SNRs in the LMC.

It is important to extend UV studies of SNRs down to the Lyman limit. Between the Lyman limit and Lyα, which is the effective lower limit to the spectral coverage of the *International Ultraviolet Explorer* (*IUE*) and the *Hubble Space Telescope*, lie several important diagnostic lines, most notably O VI λλ1032, 1038. O VI is produced in shocks with velocities greater than ~ 160 km s^{-1}. Hence, O VI probes shock waves with velocities intermediate to the shocks comprising the bright optical filaments (~ 100 km s^{-1}) and the X-ray producing main blast wave (typically greater than 300 km s^{-1} in middle-aged SNRs). For shocks with $V \sim 200$ km s^{-1}, O VI emission is a dominant emission-line energy loss mechanism in the postshock flow (cf. Raymond et al. 1983; Hartigan, Raymond, & Hartmann 1987).

Recently, Blair et al. (1991a) using *Voyager* UVS data have suggested that shocks with $V \sim 200$ km s^{-1} are spatially widespread in the Cygnus Loop. The Hopkins Ultraviolet Telescope (HUT) observed two filaments in the Cygnus Loop, both of which are consistent with shock speeds of 165–180 km s^{-1}. Blair et al. (1991b) describe HUT observations of an "incomplete" shock on the E side of the Cygnus Loop. Though the postshock flow has not recombined to neutrality, the relative strength of O VI to other high-ionization species constrains the shock velocity tightly. Long et al. (1992) present the HUT far-ultraviolet (FUV) spectrum of a "nonradiative" Balmer-dominated shock in the NE Cygnus Loop. They conclude that the results favor postshock equilibration of ion and electron temperatures but indicate that the observations may also be consistent with a decelerating shock and slower Coulomb equilibration.

In this paper, we describe the first FUV observations of an extragalactic SNR which extend to the Lyman limit. The observations were obtained with the Hopkins Ultraviolet Telescope as part of the *Astro-1* space shuttle mission in 1990 December. We discuss the observations and reductions in § 2, and we analyze these data and discuss the origin of the detected O VI emission in § 3. We briefly summarize our conclusions in § 4.

2. OBSERVATIONS

HUT consists of a 0.9 m mirror feeding a prime-focus spectrograph with a microchannel-plate intensifier and Reticon detector (Davidsen et al. 1992). The region from 830 to 1860 Å is covered in first-order at 0.51 Å pixel^{-1} with ~ 3.5 Å resolution. The N49 observation occurred on the final day of the *Astro-1* mission—1990 December 10 at 13:24 UT. The 9.″4 × 116″ aperture was placed on the bright eastern ridge of emission as shown in Figure 1 (Plate 4), with the long dimen-

[1] Center for Astrophysical Sciences, Department of Physics and Astronomy, John Hopkins University, 34th and Charles Streets, Baltimore, MD 21218.
[2] Space Telescope Science Institute, 3700 San Martin Drive, Baltimore, MD 21218.
[3] Institute of Astronomy, University of Cambridge, The Observatories, Madingley Road, Cambridge, CB3 0HA, England.
[4] Laboratory for Astronomy and Solar Physics, Code 681, NASA Goddard Space Flight Center, Greenbelt, MD 20771.

PLATE 4

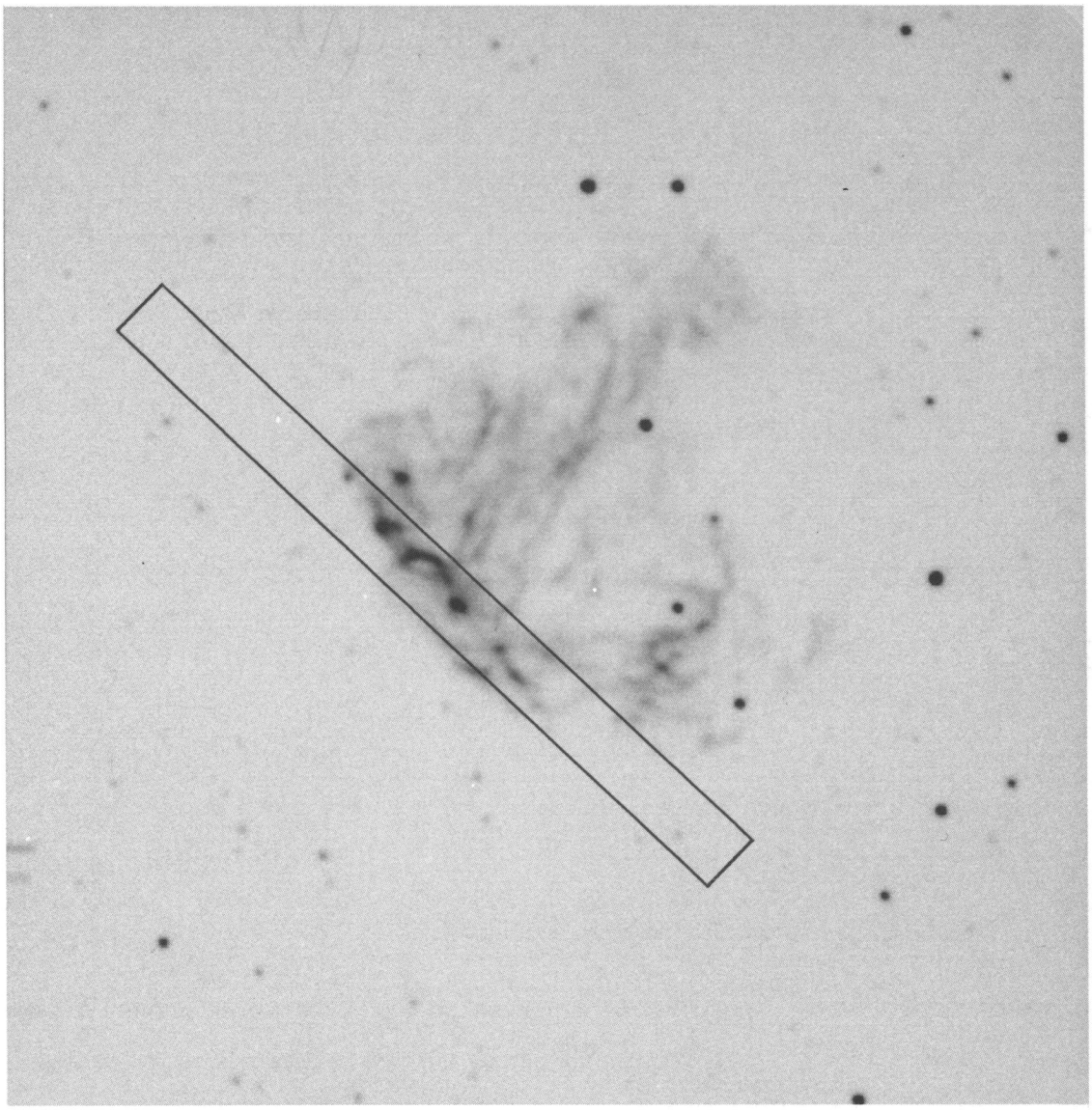

FIG. 1.—HUT aperture (9″.4 × 116″) positioned on an [O III] λ5007 image of N49. The optical image was obtained with the 2.5 m Dupont telescope at Las Campanas Observatory (see Vancura et al. 1992).

sion of the aperture at a position angle of 46°. N49 itself was not visible in the HUT acquisition camera, and the aperture was centered at $\alpha(1950) = 05^h25^m59^s.5$, $\delta(1950) = -66°07'42''$, using preplanned guide stars. The total integration time was 898 s and took place entirely during orbital day. During this time, the root-mean-square pointing error along the dispersion axis of the aperture was 3".8, somewhat larger than for most targets. The projected size of the aperture at a distance of 50 kpc is 2.28 × 28.1 pc, and no spatial information is available within the slit.

The raw HUT data were converted to IRAF[5] format to facilitate reduction and analysis. Before flux calibration, the counts data were corrected for pulse persistence in the phosphor readout, dark count background, and scattered light. As discussed by Davidsen et al. (1992), our flux calibration is based on a comparison of in-flight observations of the white dwarf G191-B2B to stellar atmospheric models in addition to pre-flight and post-flight laboratory calibration measurements.

Figure 2 shows the flux-calibrated HUT spectrum of N49, after smoothing with a boxcar filter of width 3 pixels (1.5 Å). Because the observation took place entirely during orbital day, a large number of airglow lines contaminate much of the spectral range. However, lines of O VI λ1035, O IV] λ1403, C IV λ1550, and He II λ1640 are clearly present, and Si IV λ1397 is detected marginally. We do not detect N V λ1240. We have checked for possible airglow contamination at these wavelengths by examining a pure airglow spectrum, presented also in Figure 2, obtained earlier in the mission through the same aperture. Aside from the contamination described below, there is no evidence for enhanced airglow emission at any of the wavelengths corresponding to the lines that we attribute to

[5] IRAF is distributed by the National Optical Astronomy Observatories, which is operated by the Association of Universities for Research in Astronomy, Inc. (AURA), under cooperative agreement with the National Science Foundation.

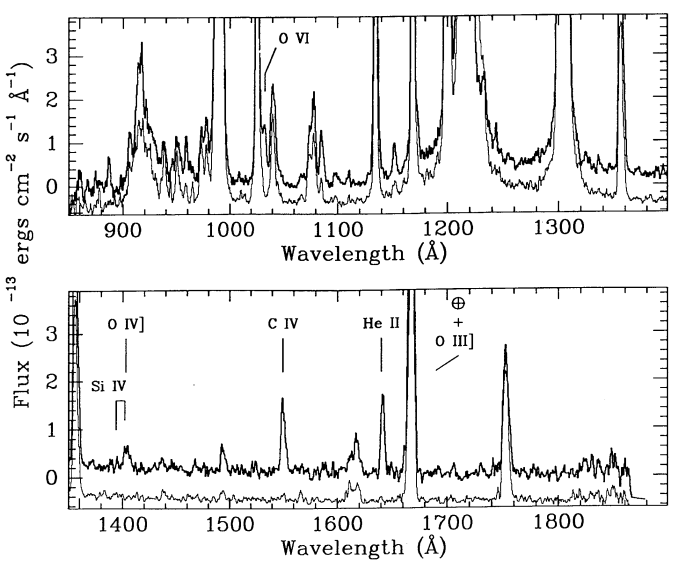

FIG. 2.—Entire, flux-calibrated N49 spectrum obtained by HUT through a 9".4 × 116" aperture, smoothed with a boxcar filter of width 3 pixels (1.5 Å). SNR lines are indicated; all other emission is due to the Earth's airglow, which is strong in this large aperture observation taken during orbital day. Offset for comparison and shown as a thin line is a pure airglow spectrum taken through the same aperture and smoothed in the same manner.

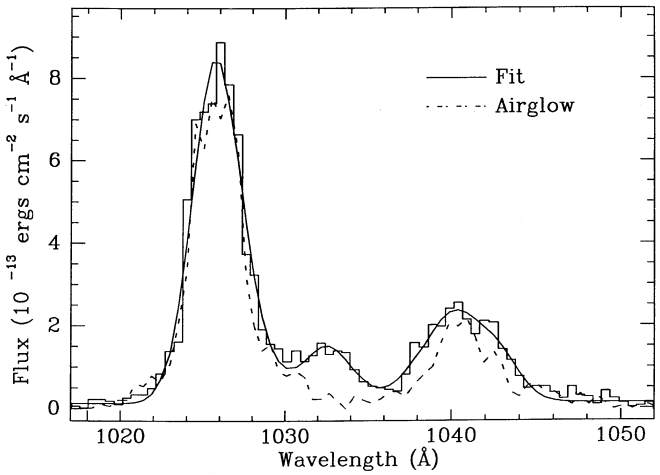

FIG. 3.—HUT N49 spectrum in the region around O VI λ1035. The unsmoothed data are presented in histogram form. For comparison, the minimum χ^2 fit and the airglow spectrum from Fig. 2 are superposed on the SNR spectrum.

N49. We have measured line fluxes in IRAF using the program "specfit", written by one of us (G. A. K.) at JHU. With the flux-calibrated spectrum and associated error array as input, we fit Gaussian profiles to the emission lines. The line flux, central wavelength, and the full-width at half maximum (FWHM), in addition to the background level, were permitted to vary freely until χ^2 was minimized. In all cases, acceptable values of χ^2 were obtained. We present observed wavelengths and fluxes in Table 1. Errors are 1 σ for the two interesting parameters of wavelength and flux.

The main importance of the HUT observation is that O VI has been detected for the first time. The portion of the HUT spectrum containing O VI is shown in Figure 3. This region is complicated by a blend of airglow emissions from Lyβ, O I λ1026, and O I λ1040. However, comparison with a pure airglow spectrum obtained earlier in the mission (superposed in Fig. 3) shows an excess of emission from N49 at ~1033 Å. There are no known airglow lines at this wavelength, and we attribute the emission to O VI λλ1032, 1038. To determine the O VI flux accurately, we fit the SNR emission and airglow lines simultaneously. The components of the O VI doublet were fixed in the optically thin 2:1 ratio, and their separation was held constant. Under these constaints, χ^2 was 63.8 for 72 data points and 14 free parameters. This should be compared to a χ^2 of 188.4 for 11 free parameters if the same wavelength region in the N49 spectrum is fit without O VI.

The strength of N V λλ1239, 1243 in N49 is difficult to determine due to contamination from terrestrial sources such as N I λ1243 and the scattering wings of Lyα. There is a faint feature at 1243.3 Å in the spectrum; this corresponds precisely to the rest wavelength of the N I airglow line. The lines of O VI and C IV show redshifts of ~200 km s^{-1} and 250 km s^{-1}, respectively. This is consistent with the redshift of the LMC, ~270 km s^{-1}, or 1.1 Å at 1240 Å. Assuming a similar redshift for N V, there should not be any N V at 1243.3 Å. Furthermore, if the λ1243 feature is the red line of the N V doublet, the blue line should be roughly twice as strong. However, there is no feature near 1239 Å, and the 2 σ upper limit to N V λ1238.8 emission between 1238.8 and 1241 Å is 7.4×10^{-14} ergs cm^{-1} s^{-1}. Assuming a 2:1 ratio for the two components, we obtain an upper limit of 1.1×10^{-13} ergs cm^{-2} s^{-1} for the total emission in both lines.

For the region around 1400 Å, we have fit the two Si IV lines and five O IV] lines simultaneously. The Si IV doublet separation was held constant, and the ratio of fluxes (λ1394:λ1403) was fixed in a 2:1 ratio. For O IV], the multiplet separation was also held constant, and the flux ratios were fixed according to the collision strengths and transition rates of Mendoza (1983).

The red component of any O III] $\lambda\lambda$1661, 1666 emission from the SNR is blended with second-order O II λ834 from the airglow. A survey of the region around λ1661 reveals a statistically insignificant excess of emission above the background. The 2 σ upper limit is 1.83×10^{-13} ergs cm^{-2} s^{-1}. Because of the large uncertainties in the λ1666 flux measurement, we have assumed that the λ1666:λ1661 flux ratio is 2.5 (Mendoza 1983) to obtain an upper limit of 6.4×10^{-13} ergs cm^{-2} s^{-1}.

Ultraviolet spectra of N49 have been obtained previously with *IUE* (Benvenuti, Dopita, & D'Odorico 1980; VBLR). There are significant variations in the UV line intensities with position. The position designated A by VBLR most closely matches the location of the HUT aperture, lying along the bright E ridge with a similar position angle. For comparison with the HUT data, we list the observed *IUE* fluxes at position A in the last column of Table 1. The observed C IV surface brightness (for the HUT slit 40% filled, see Fig. 1) is roughly the same for both *IUE* position A and the HUT position. This is consistent with both the relatively uniform optical brightness distribution of filaments along the E ridge and the close association between *IUE* and optical emission (VBLR). The HUT fluxes of Si IV + O IV] and He II relative to C IV are consistent with the range of values obtained with *IUE*. Our upper limit of N V:C IV does not improve on the results of *IUE* because of the large flux in the scattering wings of geocoronal Lyα in the HUT observation.

We correct the observed fluxes for interstellar reddening by applying the "non-30 Dor" LMC extinction curve of Fitzpatrick (1985). We take this curve to lie one-third of the way from the $A(\lambda)/E(B-V)$ Galactic curve of Seaton (1979) to the LMC curve of Howarth (1983). We adopt an average color excess $E(B-V)$ of 0.37. The observed and dereddened line intensities, scaled relative to C IV(total) = 100, are shown in Table 1.

There are spatial reddening variations along the line of sight to N49. Because blue light propagates preferentially along lines of sight with low extinction, correcting for extinction through the use of an optically derived average reddening will overestimate intrinsic UV line strengths. This is especially important for O VI. To quantify this effect, we consider a source of uniform brightness and varying extinction. We assume the probability P that a particular line of sight has a specific value of $E(B-V)$ is given by $P[E(B-V)] \sim \exp\{-[E(B-V) - E(B-V)_0]^2/[2\sigma^2]\}$, for some $E(B-V)_0$. For values of σ between 0 and 0.2, we calculated $E(B-V)_0$ necessary to produce an optically derived average $E(B-V) = 0.37$. We define the correction factor to be the ratio of actual extinction ($10^{0.4A(\lambda)}$) to that inferred for a uniform $E(B-V) = 0.37$. Defined in this way, the correction factor is a very slowly varying function of $E(B-V)_0$; effectively it is a function only of σ, except for large $\sigma \sim E(B-V)_0$, in which case the Gaussian function becomes truncated. The correction factor for several UV lines as a function of σ is presented in Figure 4. Using the long-slit spectra obtained by VBLR of the E ridge, we have extracted 2″ × 2″ square apertures and find a standard deviation of 0.14 for $E(B-V)$. (Note: If the reddening varies substantially on spatial scales smaller than 2″, σ may be higher.) Using $\sigma = 0.14$, the correction factors are 0.41, 0.67, 0.77, 0.78, 0.84, 0.85, 0.85 for O VI, N V, Si IV, O IV], C IV, He II, and O III], respectively.

Resonance line absorption within the LMC also may affect the relative line intensities. The profiles of N V and C IV absorption lines seen in LMC stars (cf. Savage & de Boer 1981; Dupree et al. 1987) suggest that a large fraction of the emission blueward of the rest velocity (in the LMC frame) will be absorbed. This absorption should be less complete away from the 30 Dor region. As a correction, we choose to multiply the resonance line fluxes by 4/3. Absorption by the Galactic halo is less significant because of the redshift of the LMC (cf. Savage & de Boer 1981) and will be ignored. The next-to-last column in Table 1 represents our best estimates for intrinsic fluxes, taking

TABLE 1

HOPKINS ULTRAVIOLET TELESCOPE OBSERVED AND INTRINSIC LINE FLUXES FOR N49

Feature	λ_0[a]	$\lambda_{observed}$[a]	$F_{HUT}(\lambda)$	$I(\lambda)$[b]	$I(\lambda)_0$[c]	$F_{IUE}(\lambda)$[d]
O VI λ1035	1031.9	1032.6 ± 0.3	123 ± 15	829 ± 101	405 ± 49	...
N V λ1240[e]	1238.8	...	< 15	< 32	< 25	< 8.3
Si IV λ1397	1393.8	1395.3 ± 1.1	16 ± 9	21 ± 12	19 ± 11	...
O IV] λ1403	1401.2	1403.6 ± 0.8	45 ± 10	57 ± 13	40 ± 9	22
C IV λ1550	1548.2	1549.5 ± 0.2	100	100	100	100
He II λ1640	1640.4	1641.4 ± 0.2	99 ± 11	89 ± 10	68 ± 8	89
O III] λ1663[e]	1660.8	...	< 88	< 76	< 58	59
C IV λ1550[f]			7.32 ± 0.79	149 ± 16	167 ± 18	3.29

[a] Rest and observed wavelengths are given for the dominant component expected in the feature. The relative separation of each of the other components was held constant.

[b] Dereddened fluxes assuming a uniform $E(B-V) = 0.37$. See text for discussion and limitations of this procedure.

[c] Dereddened (and resonance line LMC absorption corrected) fluxes assuming spatially variable reddening with $E(B-V) = 0.37$ and $\sigma = 0.14$ (see text). This is our best estimate of the intrinsic flux.

[d] Observed values for *IUE* position A from Vancura et al. 1992.

[e] Fluxes appearing with " < " represent 2 σ upper limits.

[f] Fluxes for each feature are given relative to C IV = 100. As appropriate, the observed or corrected flux in C IV in units of 10^{-13} ergs cm^{-2} s^{-1} is given at the bottom of the column.

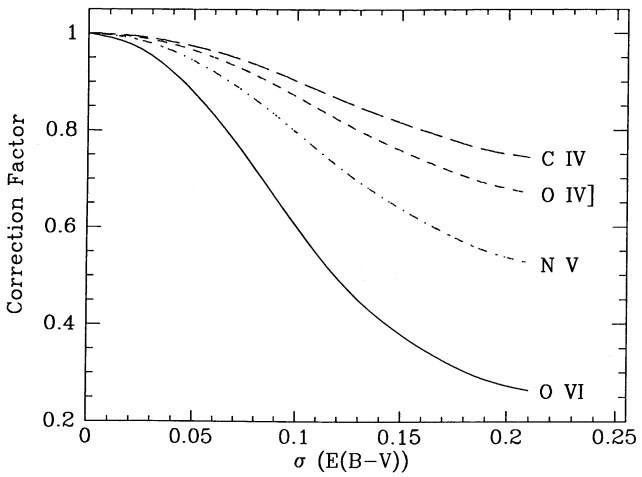

FIG. 4.—Extinction correction factor vs. σ (Gaussian σ of the assumed reddening distribution) for $E(B-V) = 0.37$. Note the largest correction is needed for O VI.

TABLE 2

COMPARISON OF HOPKINS ULTRAVIOLET TELESCOPE OBSERVATION TO MODELS

Line	Observed[a]	A_{161}[b]	A_{171}[b]	A_{190}[b]	V_1[c]	V_2[d]
O VI λ1035	405 ± 49	204	508	922	256	388
N V λ1240	< 25	49	40	42	20	24
Si IV λ1397	19 ± 11	16	17	17	26	24
O IV] λ1402	40 ± 9	85	84	74	44	50
C IV λ1550	100 ± 11	100	100	100	100	100
He II λ1640	68 ± 8	22	22	25	20	22
O III] λ1663	< 58	46	45	41	39	39

[a] Observations are taken from Table 1. Fluxes are given relative to C IV = 100. The statistical errors are shown; however the systematic error on O VI dominates the statistical error as discussed in § 2.

[b] The assumptions made in each of the models are discussed in the text. Models A are single velocity shocks.

[c] Model V_1 is Model V of VBLR, a power law of exponent −2.2 between 40 and 270 km s^{-1}.

[d] Model V_2 is the same as Model V_1 except that the area of shocks with velocities between 190 and 270 km s^{-1} has been doubled to 11.4%.

into account spatially varying extinction and LMC resonance line absorption. Though these values suffer from large systematic uncertainties, it is clear that the intrinsic O VI:C IV ratio is greater than 1.2 (the observed ratio) and is probably in the range 2–5.

3. DISCUSSION

The reason for N49's striking brightness at X-ray, UV, and optical wavelengths is that the remnant is expanding into a region in which densities (both in the intercloud medium [ICM] and the clouds themselves) are high compared to most SNRs. From multiwavelength data, VBLR inferred that an ICM density of ~ 0.9 cm^{-3} and cloud densities between 20 and 940 cm^{-3} must exist in order to match observed luminosities. They argue that a broad range of observational data on N49 can be explained by a Sedov solution in addition to which the main blast wave encounters extended clouds of the kind reporated near N49 by Hughes, Bronfman, & Nyman (1989).

To interpret the HUT data, we have used Raymond's (1979) shock code, with modifications as discussed in Cox & Raymond (1985) and the LMC abundances of VBLR, to model the emission expected from various shocks. Although, as discussed below, conditions in N49 are likely to be much more complex, we first attempted to model the data in terms of a single radiative shock. Despite the uncertainties in the O VI flux, the ratio of O VI to C IV tightly constrains the allowed shock velocity in this situation (see, e.g., Blair et al. 1991b). Assuming the ratio of O VI:C IV is in the range 2 to 5, the allowed shock velocity is between 161 and 171 km s^{-1}. Alternatively, we can attempt to use the O VI:O IV]:O III] ratios which are independent of abundance to derive the best match. In this case the best single velocity models have shock speeds between 169 and 190 km s^{-1}. We present the predicted emissions from 161, 171, and 190 km s^{-1} shocks as Models A_{161}, A_{171}, and A_{190} in Table 2, along with our best estimates of the intrinsic fluxes. None of these models fit the data very well. In particular, the model predictions for N V:C IV and O IV]:C IV are greater than observed. Assuming the abundances of VBLR are correct, no single velocity shock matches the data. If we allow the abundances to be a free parameter, then by raising the C abundance by a factor of 2, we can obtain good agreement between the HUT spectrum and a shock of velocity 190 km s^{-1}. However, the abundance of C would then be 6 times the C abundance obtained for N49 by Russell & Dopita (1990) and ≥ 0.5 dex higher than the C abundance determined for LMC H II regions (Dufour, Shields, & Talbot 1982).

An alternative possiblity is to assume that O VI is arising from shocks of higher velocity than C IV and the other lines longward of Lyα. For the abundances we have assumed, the ratio of N V:C IV is less than 0.4 for shocks with velocities ≤ 140 km s^{-1}. On the other hand, the O VI:N V ratio is ≥ 3.65 and O VI:C IV ≥ 1.80 for shock velocities ≥ 160 km s^{-1}. This suggests that O VI is mainly created in shocks with relatively high velocity ($V_s \geq 160$ km s^{-1}), while the bulk of the C IV emanates from shocks with velocities ≤ 140 km s^{-1}.

One possible source of O VI is the main blast wave. In this case, since the cooling time scale is much greater than the age of the remnant, the O VI is produced as oxygen is being ionized in the postshock gas. We have modeled the nonradiative emission from the primary shock. From VBLR, we have adopted a blast wave velocity of 730 km s^{-1}, a preshock ICM density of 0.9 cm^{-3}, and a negligible magnetic field strength of 0.1 μG. Electron collisions are the primary ionization mechanism behind the shock front. To obtain the maximum O VI flux we have assumed that the electrons and protons come to temperature equilibrium only through Coulomb interactions. Electron temperatures are thus lower than in the case where instant equilibration occurs via turbulence or other means. Each ionization zone is more extended, and this results in a greater line flux. We choose 100 yr as the point to terminate the shock's evolution. However, the truncation point is not crucial, since the ionization level of O has long surpassed O^{+5} after 100 yr.

Assuming a radius of 10 pc and a single shock covering the entire surface of N49 yields a predicted O VI flux of 8.3×10^{-13} ergs cm^{-2} s^{-1} from the main blast wave. The HUT aperture subtends $\sim 11\%$ of the surface area of the remnant, but the aperture was placed on the brightest optical and X-ray region. About 19% of the total N49 X-ray flux as observed with *Einstein* emanates from within the HUT aperture position. About 27% of the total [O III] λ5007 flux comes from the same region. Thus, we estimate that the HUT slit would have captured at most 30% of the total O VI light of N49 or 2.5×10^{-13} ergs cm^{-2} s^{-1}. This is more than two orders of

magnitude below the reddening-corrected O VI intensity (see Table 1). Different reddening or resonance scattering corrections cannot account for this large difference. We conclude that the primary blast wave is not responsible for the O VI emission.

An alternative possibility is that shocks with velocities intermediate to the optical shocks and the main blast wave are producing the bulk of the O VI. The cloud densities in N49 are sufficiently high that shocks with velocities $\lesssim 230$ km s^{-1} become radiative in $\lesssim 1200$ yr (VBLR). Echelle data support the existence of high-velocity radiative shock waves in N49; typical bulk motions of ~ 200–280 km s^{-1} are seen in [O III] $\lambda\lambda$4959, 5007 and Hα (Shull 1983; Chu & Kennicutt 1988). Pressure equilibrium dictates that only a modest factor of 2 difference in density is needed between the clouds harboring shocks of $V \sim 140$ km s^{-1} and those into which 200 km s^{-1} are progressing.

We have modeled a 200 km s^{-1} shock, traversing a cloud of density 37.5 cm^{-3}. The predicted emission of several lines as a function of time and swept-up column density are presented in Figure 5. Shocks with velocities near 200 km s^{-1} produce copious O VI emission because the postshock ionization peaks near O^{+5}. As required by our observations, O VI production dominates other high ionization lines. The ratio of O VI to C IV, for example, is about 10. For the high densities applicable to N49, the time scale for these shocks to become radiative is relatively short. From Figure 5, the cooling and recombination zone is nearly complete 500 yr after shock passage. However, in as little as 5 years, there is already abundant O VI emission at a rate ten times that of C IV. Thus the main attributes of these shocks are bright *and* dominant O VI emission in a short time after shock passage.

VBLR modeled N49 emissions by creating a grid of shock models in velocity space assuming a fixed ram pressure and scaling the preshock magnetic field to achieve constant maximum postshock density (to match the observed optical [S II] densities). They established that a range of shock velocities in N49 is necessary to explain the *IUE*, optical, and IR observations, which cannot be made to agree with any single shock velocity regardless of abundance set assumed. They found that a power-law velocity distribution of shocks between 40 and 270 km s^{-1} matched the multiwavelength data and that the bulk of these emissions arise from shocks $\lesssim 140$ km s^{-1}. Their best fit (Model V) had, for area A covered by shocks with velocity V km s^{-1}, $A(V) \propto (V/100)^{-2.2}$. In Table 2, we reproduce as Model V_1 a portion of VBLR's Model V including a prediction for O VI and Si IV. The predicted O VI is in reasonable agreement with our observed value given the uncertainties discussed above. The major difference between the model and the observation is that the model predicts too little He II λ1640. An errant He abundance is unlikely to account for the discrepancy, since the He abundance was derived by fitting two optical He I lines at λ5876 and λ6678. The disparity may be due in part to an inaccurate measure of the conversion efficiency of He II Lyβ (λ256) to He II Hα (λ1640).

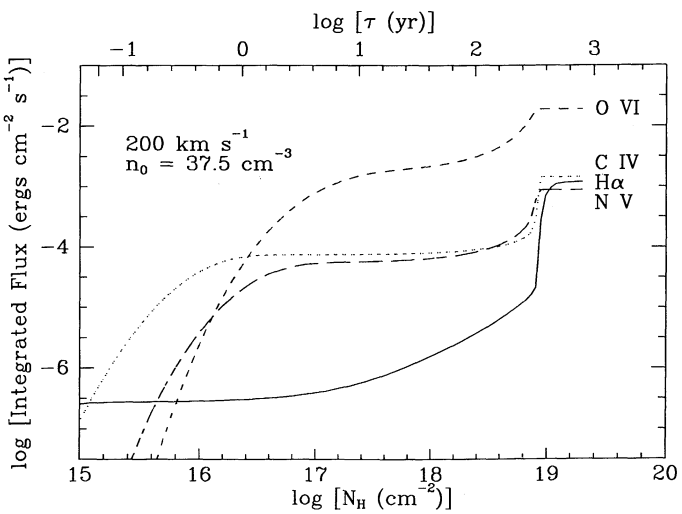

FIG. 5.—Model output of a 200 km s^{-1} shock, traversing a cloud of density 37.5 cm^{-3}, assuming Coulomb equilibration. The lower horizontal axis is swept-up column density, while the upper horizontal axis is the time since shock passage. The vertical axis is line emission in ergs cm^{-2} s^{-1} through the front of the shock. Note the dominance of O VI over other UV and optical lines.

Though the intrinsic O VI flux is quite uncertain, our best estimate indicates a somewhat higher value than that predicted by Model V_1. Because by construction the shocks producing most of the O VI contribute little to the emissions of other lines, we may go one step further in our modeling by incorporating more fast shocks to raise the relative O VI line strength. Model V_2 is identical to Model V_1 except that the surface area of shocks with velocities between 190 and 270 km s^{-1} ($n_0 =$ 20–40 cm^{-3}) has been raised from 5.7% to 11.4% of the total. This brings the predicted flux of O VI into better agreement with the estimated intrinsic flux. Aside from O VI and [Ne IV] λ2423, *all* the other emission lines modeled by VBLR remain constant to within 25%.

The actual N V emission may be considerably less than the 2 σ upper limit that we have derived. If the intrinsic N V emission is significantly below our upper limit, then there may be a deficit in the number of steady-state shocks with velocities between 150–170 km s^{-1} as compared to shocks with velocities greater than or less than these values. In this case, thermally unstable cooling (cf. Innes, Giddings, & Falle 1987; Innes 1992) or interstellar conditions may effectively create distinct shock systems. The fast shock waves producing O VI may be completely separate from the shocks producing the bright optical emission. A single power-law model of shock velocities would then not be appropriate. A better limit to the N V flux is needed to further constrain the distribution of shock velocities and the physical processes present in N49.

4. CONCLUSIONS

We have used the Hopkins Ultraviolet Telescope to obtain the first sub–Lyman-α spectrum of an extragalactic SNR, N49 in the Large Magellanic Cloud, and we have detected emission from O VI $\lambda\lambda$1032, 1038 in this spectral region. The measured fluxes of C IV, O IV], and O VI and the upper limit on N V provide stringent limits on the shocks responsible for the bulk of the O VI production. O VI cannot originate in the shocks with velocities $\lesssim 140$ km s^{-1} which are responsible for the bulk of the *IUE* UV and optical emission because the postshock temperature is not high enough. The nonradiative main blast wave cannot account for the brightness of the observed O VI emission. The majority of the O VI must originate in an optically faint system of shocks (covering much less surface area than the bright optical shocks) with velocities ~ 190 to 270 km s^{-1} and preshock densities ~ 20 to 40 cm^{-3}. The emission from such high-velocity shocks is dominated by O VI. Evidence for shocks at these velocities in N49 has been seen previously in echelle spectra (Shull 1983; Chu & Kennicutt 1988). The large

preshock densities (with the corresponding small cooling times) allow shocks at these velocities to have potentially complete cooling and recombination zones. We have fit various power-law shock velocity distributions (40 km $s^{-1} \leq V \leq 270$ km s^{-1}) to the HUT data. We find that such models can account for the observed line intensities and that the abundances derived by VBLR from *IUE* and optical data are insensitive to the presence of additional shocks with velocities between 190 and 270 km s^{-1}.

We would like to thank the Spacelab Operations Support Group at Marshall Space Flight Center for providing valuable assistance during the *Astro-1* mission. We give special thanks to the astronauts on-board *Columbia*, whose adeptness and perseverance made the success of the mission possible. We also which to thank J. Raymond for insightful discussions and for permission to adapt and use his shock code. The Hopkins Ultraviolet Telescope project is supported by NASA contract NAS 5-27000 to Johns Hopkins University.

REFERENCES

Benvenuti, P., Dopita, M., & D'Odorico, S. 1980, ApJ, 238, 601
Blair, W. P., Long, K. S., Vancura, O., & Holberg, J. B. 1991a, ApJ, 374, 202
Blair, W. P., et al. 1991b, ApJ, 379, L33
Chu, Y.-H., & Kennicutt, R. C. 1988, AJ, 95, 1111
Cline, T. K., et al. 1982, ApJ, 255, L45
Cox, D. P., & Raymond, J. C. 1985, ApJ, 298, 651
Davidsen, A. F., et al. 1992, ApJ, 392, 264
Dennefeld, M. 1986, A&A, 157, 267
Dopita, M. A. 1979, ApJS, 40, 455
Dufour, R. J., Shields, G. A., & Talbot, R. J., Jr. 1982, ApJ, 252, 461
Dupree, A. K., Kirshner, R. P., Nassiopoulos, G. E., Raymond, J. C., & Sonneborn, G. 1987, ApJ, 230, 597
Eastman, R. G., & Kirshner, R. P. 1989, ApJ, 347, 771
Fitzpatrick, E. L. 1985, ApJ, 299, 219
Hartigan, P., Raymond, J., & Hartmann, L. 1987, ApJ, 316, 323
Howarth, I. D. 1983, MNRAS, 203, 301
Hughes, J. P., Bronfman, L., & Nyman, L. in Supernovae, ed. S. E. Woosley (NY: Springer), 679
Innes, D. E. 1992, A&A, 256, 660
Innes, D. E., Giddings, J. R., & Falle, S. A. E. G. 1987, MNRAS, 226, 67
Long, K. S., Blair, W. P., Vancura, O., Bowers, C. W., Davidsen, A. F., & Raymond, J. C. 1992, ApJ, in press
Long, K. S., Helfand, D. J., & Grabelsky, D. A. 1981, ApJ, 248, 925
Mathewson, D. S., Healy, J. R., & Westerlund, B. E. 1963, Nature, 199, 681
Mendoza, C. 1983, in IAU Symp. 103, Planetary Nebulae, ed. D. R. Fowler (Dordrecht: Reidel) 143
Raymond, J. C. 1979, ApJS, 39, 1
Raymond, J. C., Blair, W. P., Fesen, R. A., & Gull, T. R. 1983, ApJ, 275, 636
Russell, S. C., & Dopita, M. A. 1990, ApJS, 74, 93
Savage, B. D., & de Boer, K. S. 1981, ApJ, 243, 460
Seaton, M. J. 1979, MNRAS, 187, 73P
Shull, P. 1983, ApJ, 275, 611
Vancura, O., Blair, W. P., Long, K. S., & Raymond, J. C. 1992, ApJ, 394, 158 (VBLR)